AIP Advances

Thrust measurement of an ion thruster by a force probe approach and comparison to a thrust balance

Cite as: AIP Advances **12**, 045218 (2022); https://doi.org/10.1063/5.0066401
Submitted: 29 November 2021 • Accepted: 21 March 2022 • Published Online: 13 April 2022

Steffen Scharmann, Konstantin Keil, Jana Zorn, et al.

View Online Export Citation CrossMark

ARTICLES YOU MAY BE INTERESTED IN

Ion thrusters for electric propulsion: Scientific issues developing a niche technology into a game changer
Review of Scientific Instruments **91**, 061101 (2020); https://doi.org/10.1063/5.0010134

Combination of optical emission spectroscopy and multivariate data analysis techniques as a versatile non-invasive tool for characterizing xenon/krypton mixed gas plasma inside operating ion thrusters
Journal of Applied Physics **131**, 053301 (2022); https://doi.org/10.1063/5.0074412

Perspectives, frontiers, and new horizons for plasma-based space electric propulsion
Physics of Plasmas **27**, 020601 (2020); https://doi.org/10.1063/1.5109141

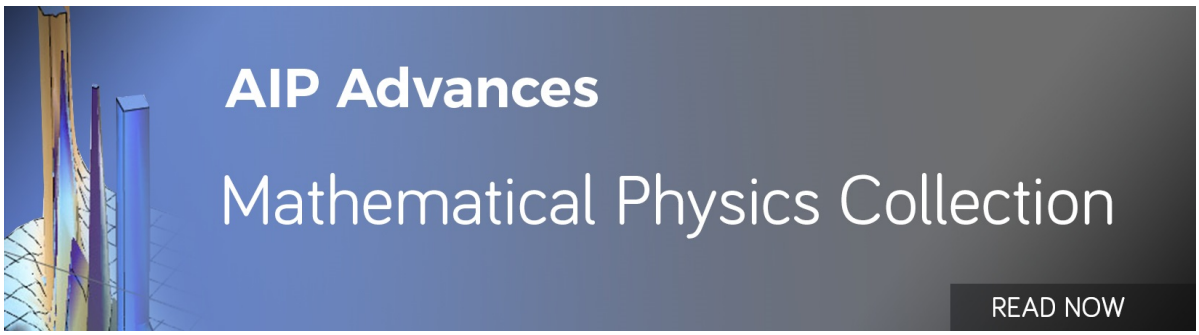

AIP Publishing

© 2022 Author(s).

Thrust measurement of an ion thruster by a force probe approach and comparison to a thrust balance

Cite as: AIP Advances 12, 045218 (2022); doi: 10.1063/5.0066401
Submitted: 29 November 2021 • Accepted: 21 March 2022 •
Published Online: 13 April 2022

View Online Export Citation CrossMark

Steffen Scharmann,[1,a)] Konstantin Keil,[1] Jana Zorn,[1] Patrick Dietz,[1] Benny Nauschütt,[1] Kristof Holste,[1] Klaus Hannemann,[1,b)] Peter J. Klar,[1] Samuel Kloss,[2] Swen Graubner,[2] Andreas Neumann,[3] and Jens Simon[3]

AFFILIATIONS

[1] Justus Liebig University Giessen (JLU), Giessen, Germany
[2] University of Applied Sciences, Giessen, Germany
[3] German Aerospace Center (DLR), Goettingen, Germany

[a)] **Author to whom correspondence should be addressed:** steffen.scharmann@exp1.physik.uni-giessen.de
[b)] Deceased.

ABSTRACT

A key parameter when characterizing the performance of an electric propulsion system is obviously its thrust. The thrust can be either determined directly using a so-called thrust balance or deduced from indirect measurements. Here, we present a comparison of thrust measurements of the same radio frequency ion thruster in the thrust range from 250 μN to 1.5 mN using three different approaches: a conventional direct measurement employing a thrust balance and two indirect measurements, one based on a force probe located stationary in the thruster's plume in conjunction with a scan of the ion beam profile using a Faraday-array scanner, and another one based on a measurement of the beam current at the grid system and a correction for beam divergence deduced from the Faraday-array scans. The results of the three approaches are compared for different beam currents, and pros and cons of the approaches are discussed.

© 2022 Author(s). All article content, except where otherwise noted, is licensed under a Creative Commons Attribution (CC BY) license (http://creativecommons.org/licenses/by/4.0/). https://doi.org/10.1063/5.0066401

NOMENCLATURE

A_g	effective exit area for the neutral particles
A_{target}	target area of the force probe
α_{div}	angle of ion beam divergence
$\beta_{sputter}$	function of $\frac{m_t}{m_p}$ and needed to calculate the sputter yield
E	ion energy
I_0	ion current
I_{beam}	beam current
I_{VC}	voice coil current
I_{target}	current on the target
$j(0)$	current density on the target of the force probe
$j(r)$	ion beam current density
J_{CEX}	neutral fast particle current resulting from CEX processes
k_{div}	correction factor for divergence effects
k_B	Boltzmann constant
l	effective path length that the ions cover
m_p	mass of the propellant
m_e	electron mass
m_{Xe}	mass of xenon
m_{Kr}	mass of krypton
m_t	mass of the target particles
M_g	mass of the neutral particles
n_g	neutral gas density
Φ_{scr}	potential on the screen grid
Φ_{acc}	potential on the acceleration grid
Φ_0	potential on the deceleration grid
q_p	charge of the propellant particles
r	radius
s_{eff}	effective displacement of the force probe

σ_{CEX}	cross section for the number of charge exchange ions
T_{ideal}	idealized thrust
T_e	electron temperature
T_N	thrust generated by the neutral particles
T/W	thrust to weight ratio
ρ	thrust per current and area
U_0	surface binding energy
U_{PS}	power supply voltage
U_{acc}	acceleration voltage
U_{tot}	effective acceleration voltage
u	unified atomic mass unit
v_{therm}	thermal speed of the neutral particles
ΔT	thrust on the force probe's target
$x_0 \backslash y_0$	distance between the mirror and the interferometric sensor before any displacement
$x_{dis} \backslash y_{dis}$	distance between the mirror and the interferometric sensor after the displacement by the hiding particles
Y	sputter yield

I. INTRODUCTION

Thrust generation to propel satellites and smaller spacecrafts in space is now routinely performed using electric propulsion systems, such as ion thrusters.[1,2] To fully characterize an electric propulsion system, measuring its thrust is mandatory. Reliable procedures and corresponding measurement equipment for determining the engine's thrust are required. Electric thrusters typically exhibit a high specific impulse but small thrusts, in the range from a few hundred mN down to μN only. The measurement of small thrusts is particularly challenging because the measurement may easily be affected by many disturbing factors either introduced by the operating thruster itself or by interference with the test environment.

The conventional approach for measuring thrust is based on sensitive thrust balances onto which the thruster is mounted during the measurement. The thrust is measured directly making use of Newton's third law, i.e., the absolute values of momentum per second of expelled propellant and force acting on the system of thruster and thrust balance are equal. Thrust balances are typically designed as a hanging, an inverse, or as a torsional pendulum.[3,4] The conventional hanging pendulum not only is the simplest configuration but also is the least sensitive to external perturbations. The resolution increases with the length of the pendulum arm, so this setup is only useful for large test facilities and is primarily used for thrusters with a high thrust-to-weight ratio, T/W.[5–7] The thrust measurement with a torsional pendulum is independent of the mass of the thruster and typically yields a higher resolution than the other two configurations.[8,9] However, due to the horizontal arrangement, a larger thruster requires stronger structures, thus lowering the sensitivity of the balance. Therefore, these torsional pendulums are typically used to characterize small thrusters with very small thrusts. Balances based on inverted pendulums are less stable but more sensitive than those based on hanging pendulums.[10,11] They allow one to perform thrust measurements in a wider T/W range. Thus, it is possible to measure the thrust of various thruster types with the same balance. Usually, balances of the inverted-pendulum type are used to measure the thrust of radio frequency ion thrusters (RITs), Hall-effect thrusters, and Kaufmann thrusters.[5] A major issue when designing a thrust balance is that the thruster mounted on the balance needs to be supplied with electric power and propellant to be operational. Undesired effects of the support lines may be manifold, e.g., their rigidity may affect the movement of the thrust balance or Joule heating of electric leads may affect the temperature stability of the balance. During operation of the thruster, additional heat sources may be present, such as the plasma burning inside a discharge vessel and emitted electromagnetic radiation, e.g., the rf-field in the case of radio frequency ion thrusters (RITs), may interfere with the measurement electronics of the balance. The test environment may also have a disturbing impact, e.g., vibrations of the pumping system of the vacuum chamber or interaction of the chamber wall with the thruster's plume.

Force probes that are placed in the ion plume of a thruster may offer an alternative to thrust balance measurements.[12] A force probe basically consists of a pendulum that is deflected by the momentum transfer of the impinging beam particles and whose displacement is measured by one or two interferometric sensors.[13] Instead of measuring the force of the thruster, the momentum transfer of the ion beam onto a target is measured. Thus, the thrust is not measured directly but deduced from the local force probe measurement and the characteristics of the ion plume under the assumption that Newton's third law holds. Advantages over a thrust balance are the opportunity of conducting spatially resolved incremental thrust measurements and of avoiding effects of the electrical and propellant feed lines on the thrust measurement itself. As the force probe is not only sensitive to charged particles but also to neutral particles, charge exchange effects inside the plasma or between the grids of a gridded ion thruster will not affect the thrust measurement.[12] We used the following approach to assess the thrust of the ion thruster using the force probe. We measured a thrust increment locally with the force probe. This result is then combined with a measurement of the 2D beam profile (e.g., with a Faraday-array-scanner), which enables us to extrapolate from the thrust increment to the thrust of the full plume. Furthermore, in the case of gridded ion thrusters, the total beam current can be measured at the grid system. The current value measured can be related to the thrust generated by the ion thruster, if the ion energies and beam divergence are known. It is worth noting that the direct thrust measurement with the thrust balance and the indirect approach with the force probe are very different in terms of possible sources of measurement uncertainty. In the former direct approach, the main sources are stiffness of the supply lines, thermal issues, and positioning of the thruster on the balance. In the latter indirect approach, issues are microscopic interaction between the ion beam and the target material as well as with the residual gas inside the vacuum test chamber and accurate knowledge of the beam profile. Thus, comparing indirect and direct thrust measurements of the same thruster under the same operational conditions comprises the ultimate test of the "approaches'" reliability. In this paper, we compare total thrust measurements using all three approaches. In all measurements, the same thruster is employed, i.e., a gridded ion thruster. Gridded ion thrusters are well suited for such a comparison because the beam current and beam energy can be accurately defined and the divergence angle of the plume is usually less than 20° and can be easily determined.

© Author(s) 2022

II. EXPERIMENTAL SETUP

A. Thruster

The RIT-4 thruster used for the experiments is a laboratory model built for validating of diagnostics or to serve as a sputter source for materials processing. The number denotes the diameter of the ion extraction grid. The ion source used is described in detail in Ref. 14. It is not optimized for power efficiency and maximum thrust but exhibits similar plume characteristics as a RIT designed for space applications. It possesses a cylindrical discharge vessel (4.3 cm in diameter and 4.1 cm in length) and an induction coil with six windings. This RIT-4 possesses a three-grid system. The first grid in contact with the plasma is called the screen grid. It is typically set to a high positive potential ϕ_{scr}. The second grid is called the acceleration grid and set to a negative potential ϕ_{acc}, which is typically in the order of 10% of the screen grid potential. The third grid connected to the thruster body serves as electrical ground potential $\phi_0 = 0$ V and should prevent back-streaming of charge-exchange ions. The net acceleration voltage of the grid for ions is $U_{acc} = \phi_{scr} - \phi_0$. The acceleration voltage of a radio frequency ion thruster is additionally increased by the plasma and floating potential[15] inside the discharge vessel so that the effective acceleration voltage U_{tot} is given by

$$U_{tot} = U_{acc} + \frac{k_B T_e}{2e} \times \left(1 + \ln\left(\frac{m_p}{2\pi m_e}\right)\right), \quad (1)$$

where T_e is the electron temperature of the propellant plasma inside the discharge vessel, m_p is the mass of the propellant particles, and m_e describes the electron mass. In our experiments, we determined the plasma bulk potential to be 45 V relative to the screen grid potential of 1000 V, resulting in an ion energy of 1045 eV for singly charged ions. In total, the grid system has 151 extraction channels whose beamlets form the ion plume generating the thrust. As we are mainly interested in comparing different approaches of measuring thrust, we set the potential ϕ_0 of the third grid to facility ground. Thus, we did not need to employ a neutralizer in the experiment.

B. Thrust balance

The thrust balance is based on the concept of a double-armed inverted pendulum as shown in Fig. 1. When operating the thrust balance, the pendulum of the balance is kept actively in its zero position. For this purpose, the deflection of the pendulum arm is detected by an interferometric sensor. In case the pendulum arm starts to move due to the operation of the thruster, the corresponding signal is passed on to a proportional–integral–derivative (PID) controller controlling a voice coil. The voice coil then counteracts the deflection of the pendulum arm. The permanent magnet of the voice coil is attached to the pendulum part (i.e., the balance table that carries the thruster) of the thrust balance and the coil of the voice coil is attached to the load-bearing part (i.e., the balance body), which does not move. The necessary current to keep the balance in its zero position is proportional to the force exerted by the thruster on the balance, i.e., the thruster's thrust. The maximal sensitivity of this method depends strongly on the stability of the measurement system. Therefore, it is important that the system is as stable as possible to external influences. In order to improve stability, the balance can be loaded with counterweights that stabilize the system; in addition, an eddy current brake is mounted for passive damping of vibrations. The thrust balance can be calibrated by using calibration weights. Different masses are attached to the thrust balance via a pulley system, and the voice coil current required for compensation is determined. The results of the calibration are shown in Fig. 1. The fit curve is given by the following equation:

$$\frac{F(I_{VC})}{N} = (1.543 \pm 0.055)\,\frac{I_{VC}}{A} - 6.123 \times 10^{-3}, \quad (2)$$

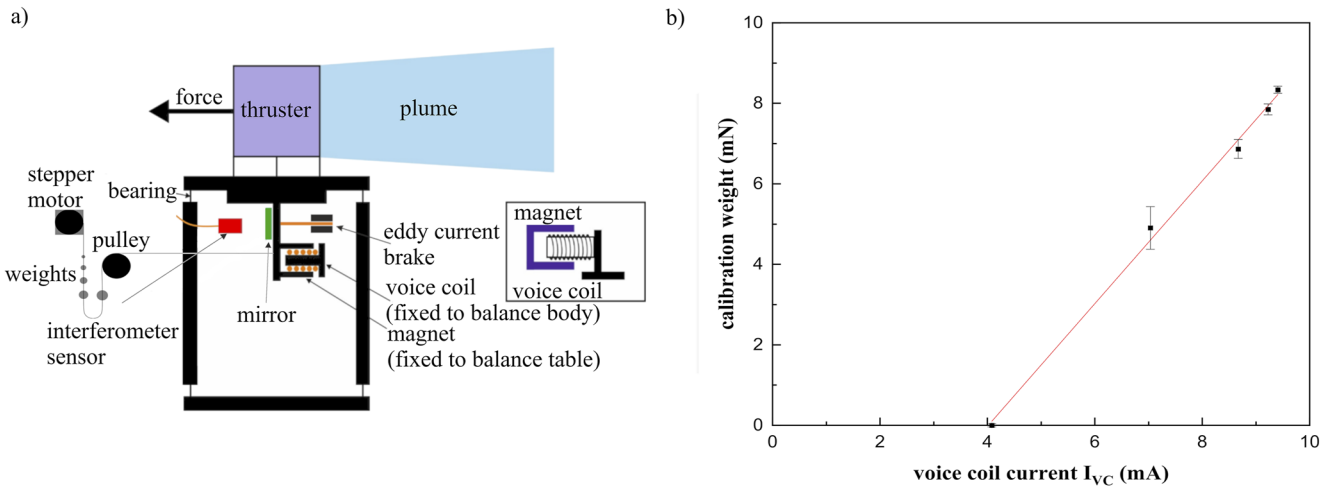

FIG. 1. (a) Schematic drawing of the inverted pendulum thrust balance. (b) Force calibration results obtained using the pulley system to apply different masses: A linear dependence of calibration weight vs voice coil current is observed. The measurement uncertainty for the calibration of the thrust balance results from the accuracy of the current source (20 μN), the accuracy of the calibration weights (2 μN), and the rolling friction of the ball bearing (8 μN) over which the thread with the calibration weights is transferred. However, because these uncertainties are all small compared to the maximum deviation from the straight line fit, it seems more appropriate to estimate the measurement uncertainty above.

© Author(s) 2022

where I_{VC} is the voice coil current. Because the thrust balance with the mounted thruster is never perfectly balanced, a non-zero constant current through the voice coil is needed to hold the balance in its zero position even without thruster operation. This is the reason for the offset in Eq. (2). This offset value can be treated as a constant. The resolution of the thrust balance depends mainly on the complete setup and the resolution of the current source used for operating the voice coil. In addition, it depends on how many supply lines are needed and how rigid they are. Furthermore, the thrust-to-weight ratio of the thruster and facility effects matter, e.g., how much the tank vibrates during operation and numerous other external disturbance factors. Many of these disturbances are difficult to quantify. From the uncertainties of the weights used for the calibration with the pulley system, we estimate an uncertainty of $2\mu N$, friction of the ball bearing yields $8\mu N$, and the current resolution of the current source used in the PID control of the voice coil yields $20\mu N$. Because of the stiff thread, it is not certain that the bottom weight will hang completely vertically on the push scale side. Assuming that the weight hangs at an angle of 25° in the rounding of the thread, this results in an error of about 10% for the bottom weight.

C. Force probe

The force probe used is based on that described in Ref. 13. A schematic drawing is depicted in Fig. 2(a). The force probe consists of a 1 mm thick and 250 mm long ceramic rod that is attached with its upper end to the housing frame in order to fix its position, i.e., to suppress rotation of the rod. At the lower end of the ceramic rod, a circular target with 20 mm diameter and a target area A_{target} = 315 mm^2 is attached, which is moved of its equilibrium position when a force acts on the target. For an accurate thrust measurement, it is important that the momentum p of the impinging particles is completely transferred on to the target and, in particular, that reflection of the impinging particles is avoided as it may lead to a larger momentum transfer (up to $2p$). Using porous graphite with a low sputtering yield and an open pore structure, where the particles enter the target but cannot leave it, should minimize reflection from the target.[16] Accordingly, we used a graphite target with an unsealed pore structure. The deflection of the target and ceramic rod from their equilibrium position is measured by two interferometric sensors from Attocube with a Fabry–Pérot interferometer (IDS 3010), which provides a displacement resolution of 2 nm in vacuum. For this purpose, a triangular mirror arrangement [shown in Fig. 2(a)] with two mirrors at right angle is attached to the ceramic rod. This type of measurement enables one to determine the direction of the incident particles by determining both components of the particles' momentum, parallel and vertical to the target surface. With

$$s_{eff} = \sqrt{(x_0 - x_{dis})^2 + (y_0 - y_{dis})^2}, \tag{3}$$

the effective displacement s_{eff} can be calculated, where x_0 and y_0 are the distance between the mirror and the sensors before any displacement. The parameters x_{dis} and y_{dis} describe the displacement after the first particles impinge on the target. Correspondingly, the measured distance is shortened, so we measure in the direction of the thrust beam. The absolute deflection distance is then calculated from the position's deviation from the zero position, which increases with increasing force. Summing over all impinging particles per time

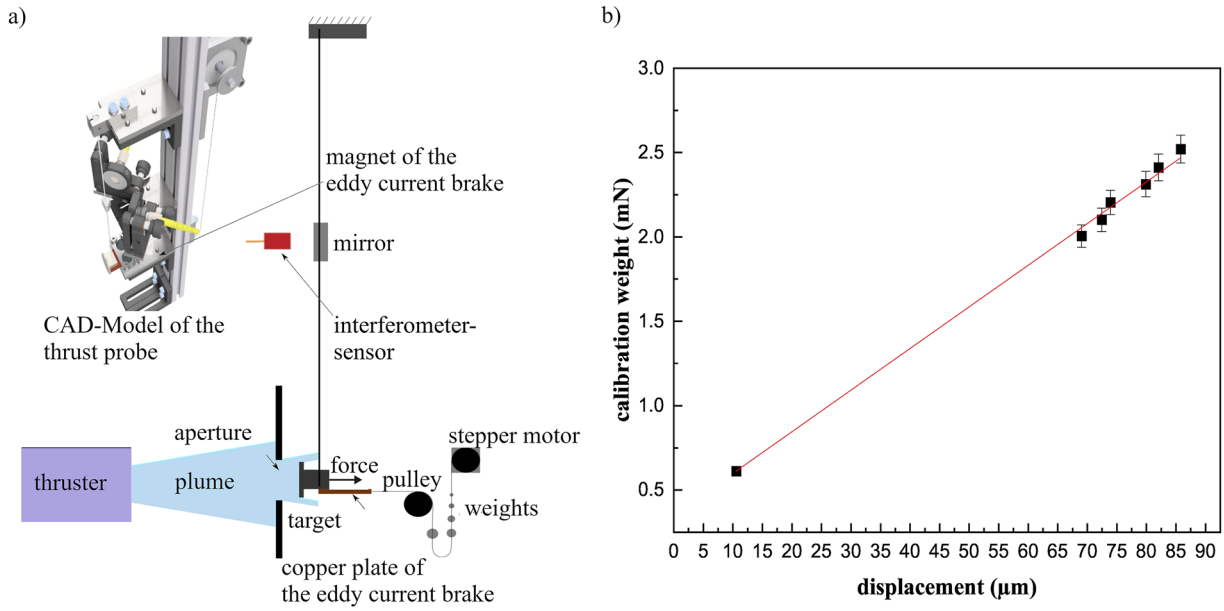

FIG. 2. (a) Schematic drawing of the force probe setup. (b) Calibration results of the force probe obtained employing the pulley system to apply different masses. A linear dependence of calibration weight vs target displacement is observed. For the calibration of the force probe, calibration weights with an uncertainty of 10 μN were used. A further source of uncertainty is the friction of the ball bearing, which could be estimated with about 10 μN. As we cannot rule out additional sources of uncertainty and judged by the statistical fluctuations, we give error bars of 40 μN in the corresponding graph.

© Author(s) 2022

interval yields the corresponding thrust increment ΔT. In order to minimize charging effects and to enable a measurement of the electric current on the target I_{target}, the conductive graphite target is contacted with a wire that passes through the insulating ceramic rod. When measuring the impinging current on the target, it is important to note that the target does not provide a repelling electrode to push secondary electrons back on to the target or to prevent electrons from the chamber from hitting the target and interfering with the current measurement result. The ion induced secondary electron emission yield is 0.1 for 1000 eV xenon ions hitting a graphite target.[17] Therefore, the maximal uncertainty for the current measurement on the target is ~10%. Assuming that secondary electrons are generated within the porous target material and that these electrons are very likely to remain inside the target, it can be assumed that the actual uncertainty is significantly below this value.

Furthermore, electric wiring allows one to change the electric potential of the target with respect to the electrical ground and, thus, yields an energy selective detection of ions impinging on the target, if desired. An eddy current brake dampens system oscillations without friction and thus increases the resolution of the system.

To enable an *in situ* calibration of the force probe, a thread is attached to the copper plate of the eddy current brake. The thread is then guided over a deflection roller. Using a pulley, as shown in Fig. 2, different weights can be used to mimic a force on the target and, thus, to establish a correlation between the exerted force and target displacement. In addition, there is an offset of the displacement at the equilibrium position of the pendulum (corresponding to zero force on the force plate) given by the distance between the mirror and the interferometric sensor. This offset can be measured very accurately and is included in the linear fitting. After moving the force probe to a new position, e.g., on a linear stage, the force probe must be recalibrated because the actual position of the entire measurement system itself has a significant influence on the zero position (offset) of the force probe's pendulum in Eq. (4). Thus, performing the calibration procedure *in situ* is essential, particularly when attempting to perform spatially resolved thrust measurements.

Figure 2(b) shows the result of the absolute mass calibration. The data points can be fitted by a linear function,

$$\frac{F(s_{\text{eff}})}{\text{N}} = (24.98 \pm 0.310)\,\frac{s_{\text{eff}}}{\text{m}} + 3.338 \times 10^{-4}, \tag{4}$$

where s_{eff} denotes the effective displacement measured by the two interferometric sensors. With this function, one may convert the measured displacement into the force acting on the target. It is worth noting that the good fit $(\pm 0,310\,\frac{\text{N}}{\text{m}})$ to the data points obtained with weights on the pulley system including that denoting the zero-position of the pendulum to a linear dependence confirms that Hooke's law is still justified in this range of displacements. This is anticipated as the relative displacement due to the bending of the rod with respect to the suspension point is rather small. Considering that the suspension point is 125 mm away from the mirror position and the maximum displacement of the mirror in the calibration process is less than 0.1 mm, the maximum relative displacement itself is less than 0.1%. The distance between the RIT-4 grid system and the probe in the actual thrust measurement was l = 323 mm. The probe was centered in front of the thruster so that the incoming particles should hit the target at normal incidence.

The offset of Eq. (4) corresponds to the distance between the interferometer head and the mirror surface. This experimental parameter can be treated as a given constant in what follows. As it is very accurately determinable, fitting the experimental data of calibration weight vs displacement by Eq. (4) (treating the displacement for zero weight as given) yields the force constant of the force probe $k \pm \Delta k = (24.698 \pm 0.310)\,\frac{\text{N}}{\text{m}}$. Error propagation yields $\frac{\Delta F}{F} = \frac{\Delta k}{k} + \frac{\Delta s_{\text{eff}}}{s_{\text{eff}}}$. Using the smallest displacement s_{eff} = 100 nm from Fig. 2 and the accuracy given by the interferometer's manufacturer for measurements in vacuum of Δs_{eff} = 2 nm, one obtains $\frac{\Delta F}{F}$ = 3.3 %. This value contains the calibration mass uncertainty $\frac{\Delta m}{m}$ of about 0.1%. We have to add an uncertainty due to friction effects within the pulley system, as discussed above. Therefore, we use a value of $\frac{\Delta F}{F}$ of 10% in what follows.

D. Faraday array

The Faraday-array scanner used for the beam profile measurement is shown in Fig. 3. The array consists out of 53 Faraday cups arranged over a distance of 1 m in the y-direction. The spacing between adjacent cups varies, such that in the center of the array, a spatial resolution of 12.5 mm is reached, and, at the periphery, the spatial resolution is about 25 mm, as shown enlarged in Fig. 3(a). The whole array is mounted on a x–z-stage and can be moved 0.95 m in the x-direction and 0.8 m in the z-direction. The maximum ion current density that can be measured using this array is 159 $\frac{\text{A}}{\text{m}^2}$ with a resolution of 5 $\frac{\text{mA}}{\text{m}^2}$. Thus, it is possible to measure the beam profile of a wide range of thruster types, for example, from a small RIT thruster, similar to the one used, up to larger RITs with grid diameters of about 30 cm with total beam currents in the 1 A-range or corresponding Hall thrusters, Kaufman-type thrusters, and HEMPTs. As an example, the intensity plot in Fig. 3(b) shows a current profile of the RIT-4 used. The divergence angle α can be determined by the two distribution functions in the x- and y-directions, knowing the distance $z = l$ to the thruster; see also Fig. 5 and the corresponding discussion. The Faraday cups of the Faraday array are always oriented parallel to the nominal ion beam direction. Thus, when a cup is off center of the beam, the ions enter it at a certain angle. This makes the effective inlet area of the cup smaller. This effect must be taken into account when evaluating the results from the Faraday measurements and is corrected for in the data presented. The distance between the RIT-4 grid system and the Faraday array in the actual thrust measurement was l = 323 mm.

E. Vacuum test chamber

All the thrust measurements were performed in the test facility "BigMac-Evo." This vacuum chamber has a diameter of 1.6 m and a length of 3.2 m. The pumping system reaches a pumping speed of about 34 000 l/s for xenon and 43 000 l/s for krypton. A basis pressure of 2×10^{-7} mbar can be reached by using one turbomolecular pump (Pfeiffer ATH 2802) and two cryopumps (Leybold CP 120-T).

III. MEASUREMENT

A. Characterization of the local force probe system

The functionality of the force probe has been tested with the RIT-4 ion thruster. For this purpose, the force probe was installed

© Author(s) 2022

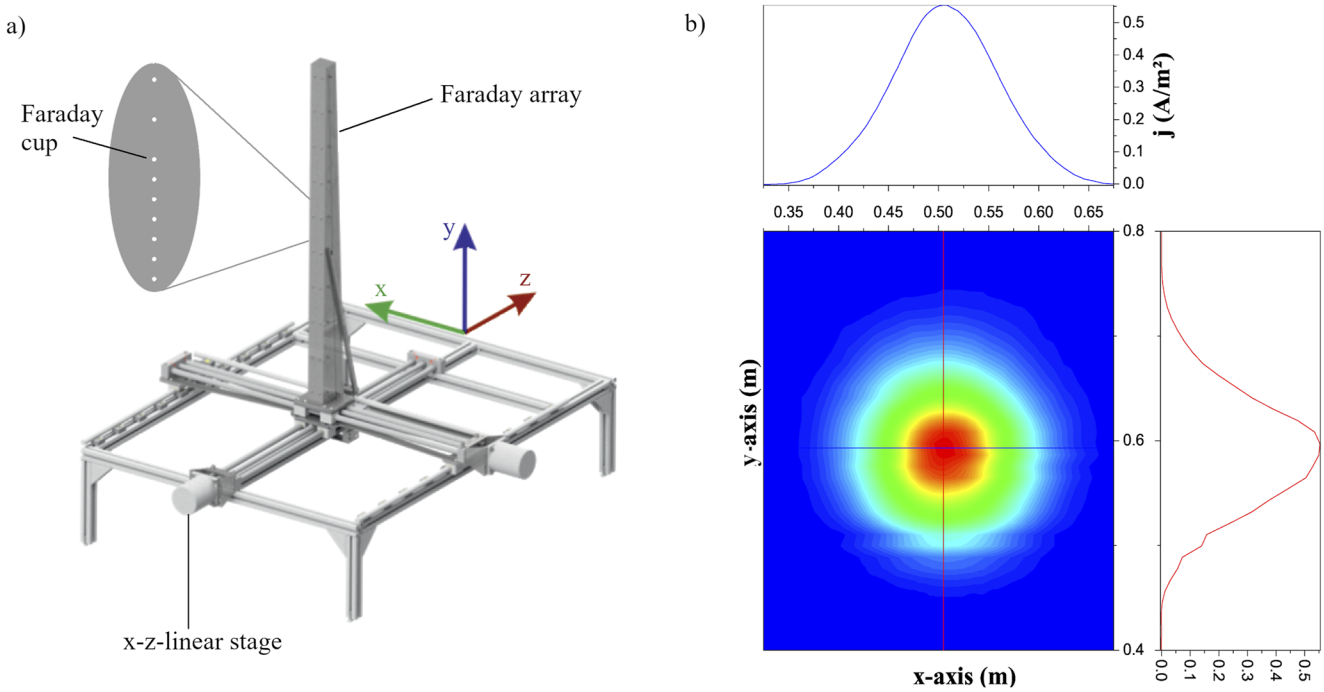

FIG. 3. (a) CAD-drawing of the Faraday-array-scanner for 3D-beam profile assessment. (b) Intensity beam profile plot of a RIT-4 operated with Xe.

together with the thruster inside the vacuum tank BigMac-Evo. The thruster was operated either with xenon or krypton as a propellant in order to study the performance of the force probe for different types of ions. In particular, we performed the measurements with both propellants using the same target currents at approximately the same ion energies. Figure 4 shows the results of local thrust measurements where the force probe was positioned in the center of the ion beam of the RIT-4. During the measurement, the beam current of the ion thruster is increased, leading to an increase of the target current. The deflection of the target as function of the target current is depicted in Fig. 4. The data reveal that the deflection of the probe varies linearly with the target current. The range of target currents corresponds to beam currents between 5 and 25 mA. During the entire measurement process, the potential of the screen grid was kept constant at ϕ_{scr} = 1000 V and the potential of the acceleration grid at ϕ_{acc} = −150 V. The beam current was adjusted by the RF-power only. As a consequence, the energy distribution of the ions impinging onto the target is virtually constant. Thus, the sputtering rate per ion and the probabilities of reflection and absorption of an impinging ion do not change with the beam current in this setting.

The second curve depicted in the graph of Fig. 4 is the outcome of the measurements using Kr as a propellant with the same voltages applied to the grid system as in the case of Xe. The thrust generated by the RIT-4 assuming ideal behavior is given by

$$T_{ideal} = I_{beam} \times \sqrt{\frac{2 \times m_p \times U_{tot}}{q_p}}, \quad (5)$$

where m_p and q_p are the mass and charge of the propellant used, respectively. As q_p = +e for both Xe and Kr and U_{acc} = 1000 V is the same in both experiments, the plasma potential differs only slightly. U_{tot} should be almost the same for both propellants, and thus, the ratio of the thrusts with Xe and Kr at the same beam current

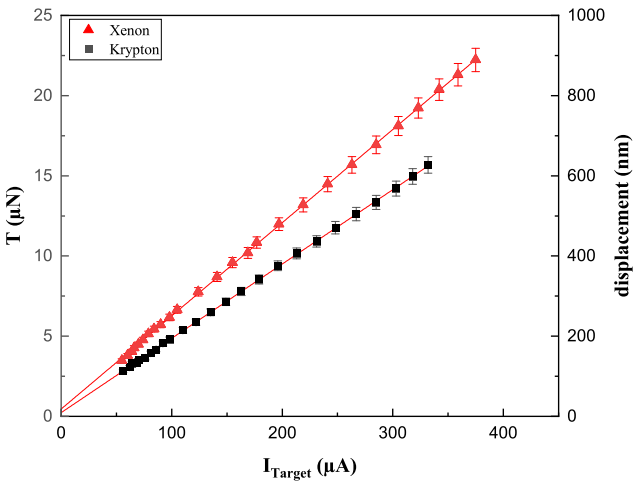

FIG. 4. Force on the probe and displacement as a function of the current on the probe comparing Xe (red triangles) and Kr (black squares) as a propellant. The error bars are calculated by error propagation from the uncertainty of the fit line.

© Author(s) 2022

should scale with $\sqrt{m_{Xe}/m_{Kr}} \backsimeq 1.252$. Despite the linear relationship between the total beam current and the target current on the force probe, the ratio of the thrust increments ΔT in the case of Xe and Kr as a propellant measured at the same target current need not necessarily scale with $\sqrt{m_{Xe}/m_{Kr}}$, even when the same beam profile is assumed (in concordance with the experiment, see the discussion of Fig. 5). The reason is that the interaction of the propellant ions with the target of the force probe may be different for Xe and Kr. The force acting on the target may arise due to contributions of different microscopic processes that differ in terms of momentum transferred to the target per ion. In particular, these are given as follows:

1. Ions of momentum p being absorbed inside the bulk of the target or its pore system, yielding simply a full momentum transfer from ion to target.
2. Ions being reflected by the target. As the microporous surface of the target is not atomically flat, the reflected ions will be reflected under various angles. However, for normal incidence, the maximal momentum transfer in the reflection process is $2p$. However, performing corresponding simulations using the SRIM (stopping and range of ions in matter) software package suggests that reflection of ions can be neglected when using graphite targets in agreement with previous work.[16]
3. Ions of momentum p sputtering atoms off the target. This process can be very complex. Furthermore, the sputter yields Y for Xe (0.176)[18] and Kr (0.35)[18] are different. For ion energies $E < 1$ keV, it holds[19]

$$Y = \frac{3}{4\pi^2} \frac{4m_t \times m_p}{(m_t + m_p)^2} \times \beta_{sputter} \times \frac{E}{U_0}, \tag{6}$$

where m_t denotes the target atom mass, β is a function of $(\frac{m_t}{m_p})$, and U_0 is the surface binding energy. Assuming that β is constant, the equation yields $Y_{Xe}/Y_{Kr} \approx 0.7$, i.e., the sputtering yield of Kr is larger than that of Xe.

4. Neutral propellant atoms hitting the target with an average velocity given by the thruster's operation temperature. The contribution to the total thrust generated by the neutral propellant atoms exiting the thruster is given by[20]

$$T_N = \frac{1}{4} n_g \langle v_{therm}^2 \rangle A_g m_p, \tag{7}$$

where n_g is the density of the neutral particles leaving the grid system, $\langle v_{therm}^2 \rangle = \frac{3k_b T_0}{m_p}$ is the average of the velocity squared of the neutral gas particles, A_g is the outlet area of the neutral particles from the grid system, and m_p is the mass of the gas particle, i.e., propellant atom. An estimate shows that this contribution is negligible in the case of the RIT-4 used in the experiment. For an operating point with 5 mA beam current, 0.24 mg/s xenon, and $T_0 = 400$ K temperature of the thruster, the contribution to the total thrust generated by the neutral gas is only about 3 μN. This is just 1% of the total thrust of about 260 μN measured at this beam current (see Fig. 6).

Nevertheless, the ratio of the slopes of the two linear dependences of thrust increment to the target current of

$$\frac{b_{Xe}}{b_{Kr}} = \frac{58.175 \frac{nN}{\mu A}}{46.400 \frac{nN}{\mu A}} = 1.254 \tag{8}$$

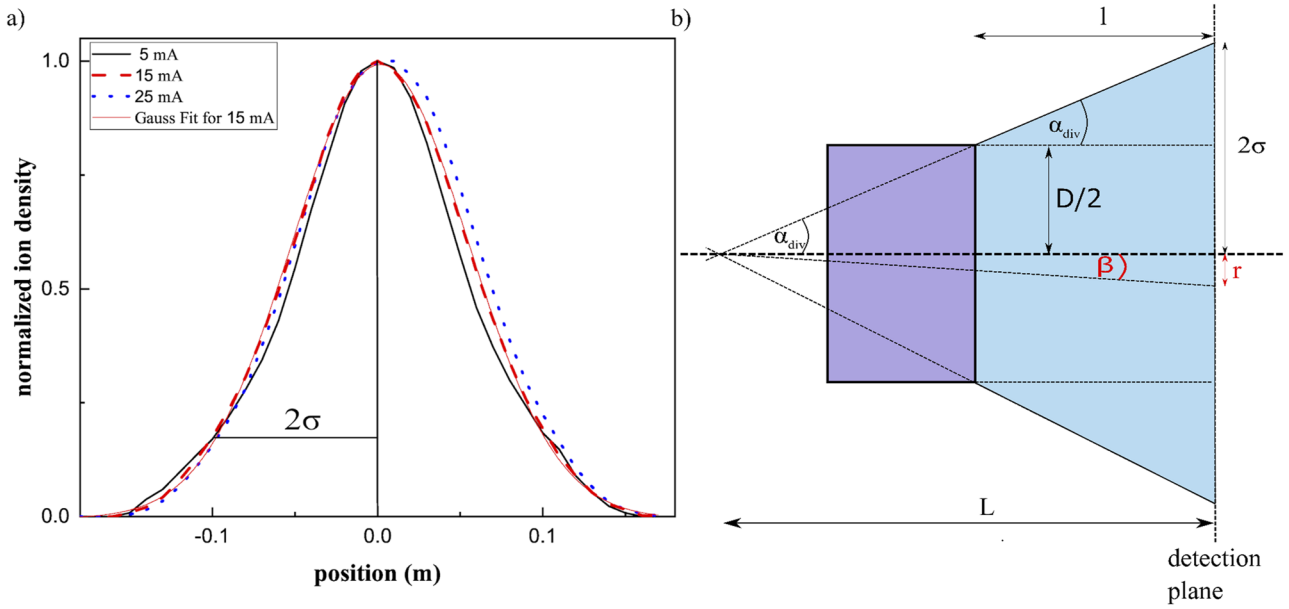

FIG. 5. (a) Beam current density as function of the Faraday array position for different beam currents with xenon at a beam current of 5 mA (black line), 15 mA (red dashed line), and 25 mA (blue dots). (b) Schematic drawing of the divergence angle principle.

© Author(s) 2022

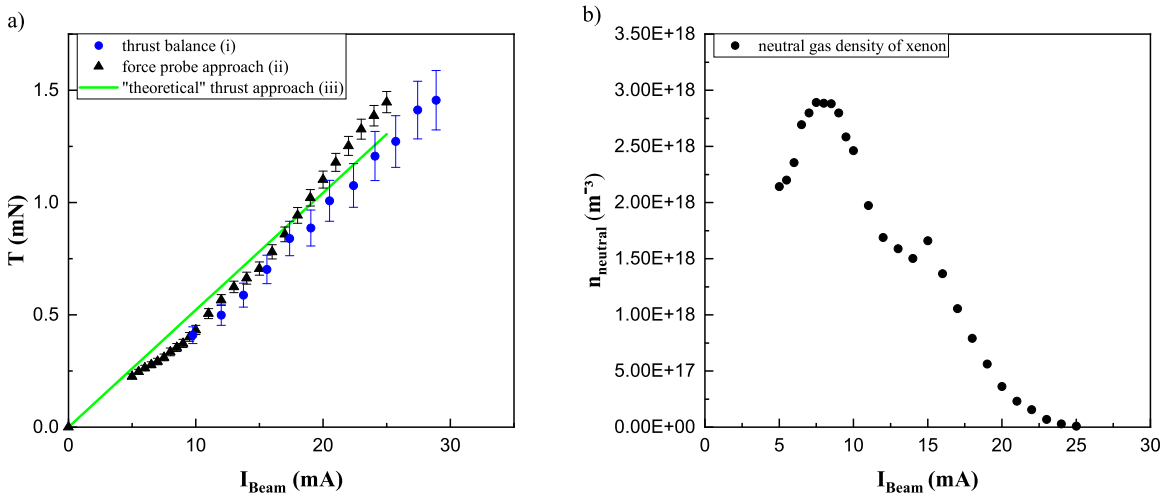

FIG. 6. (a) Comparison of the thrust balance (blue dots) and thrust probe (black triangles) measurements with the theoretical thrust (green line) vs beam current. (b) Average neutral gas density between the grid system and the force plate as a function of beam current and the neutrals between the grid and the detection system cause CEX effects.

almost matches $\sqrt{m_{Xe}/m_{Kr}} \simeq 1.252$. This suggests that the microscopic processes (3) and (4) are of minor importance in this range of ion energies as the sputtering yield differs significantly for Xe and Kr ions impinging on the target. As pointed out above, SRIM simulations suggest that that ion reflection is negligible. Thus, the ions impinging on the target are basically all absorbed, i.e., the momentum transfer per ion is p.

However, when measuring the electric current at the target, induced by the ions hitting the target, it must be taken into account that not all ions leaving the thruster and being directed on to the target will contribute to this current. If ions collide with neutral propellant particles after exiting the grid, charge exchange (CEX) may occur between the collision partners. Afterward, the now uncharged atom flies with the same speed toward the target and transfers the same momentum as it would have done as ion. However, it does not contribute to the current measurement at the target at distance l from the thruster. As a result, the total beam current $I_{beam}(z = 0)$ exiting the grid system of the thruster and the integrated beam current $I_{beam}(z = l)$ derived from the beam profile at distance l from the thruster in the direction z of the beam (where the force probe or the Faraday array are located) will differ. It holds approximately

$$I_{beam}(z) = I_{beam}(z = 0)\exp(-\sigma_{CEX} n_g z), \tag{9}$$

where σ_{CEX} is the cross section for the CEX process between a propellant ion and a propellant neutral and n_g is the average neutral propellant density in the ion beam. It is estimated to be 7×10^{17} m^{-3}. The cross section for CEX from single charged ions to neutral atoms are known, for krypton with 1000 eV ion energy $\sigma_{CEX}^{Kr} = 36.6 \times 10^{-20}$ m^2 and for xenon with the same energy $\sigma_{CEX}^{Xe} = 46.5 \times 10^{-20}$ m^2.[21] Doing the numbers, one finds that $l = 0.323$ m is only a small fraction of the mean free path for the CEX process $l_{CEX} = (\sigma_{CEX} n_g)^{-1} = 3.1$ m for Xe (3.9 m for Kr). Therefore, the particle flux of fast neutral atoms J_{CEX} generated by CEX between neutrals in the beam and ions can be approximated by the following formula[22] where a Taylor-expansion of the exponential function up to first order was used:

$$\begin{aligned} J_{CEX}(z = l) &= \frac{1}{e}\left(I_{beam}(z = 0) - I_{beam}(z = l)\right) \\ &\approx (\sigma_{CEX} n_g l)\frac{I_{beam}(z = 0)}{e}, \end{aligned} \tag{10}$$

where e is the elementary charge. In the case of our experiments, the flux of CEX neutrals amounts to roughly 10% of the original ion flux of the beam. This means that the ion current measured on the force probe is significantly reduced, i.e., $I_{target} = (I_0 - e \times J_{CEX})$ and the effect needs to be accounted for when determining the thrust using the force probe approach.

It is worth noting that it is possible to detect target current changes down to 4 μA in the force probe measurement. Such a change in the target current corresponds to a beam current variation by 0.5 mA, at an acceleration voltage of 1000 V. Under these operating conditions, this results in a force change on the target of about 0.2 μN. It is not possible to measure such small thrust variations with the thrust balance used. The smallest thrust increment resolvable by the thrust balance used is about 250 μN, i.e., more than three orders of magnitude larger.

B. Comparison of three approaches for measuring thrust

We will now attempt to determine the total thrust by three different approaches: (i) using the thrust balance, (ii) using the force probe measurement combined with a scan of the beam profile, and (iii) based on the beam profile and a corresponding correction of the ideal thrust given by Eq. (5).

- *Approach* (i) was conducted in a straightforward fashion as described in Sec. II B. The corresponding data of thrust vs

© Author(s) 2022

beam current measured at the grid are plotted in Fig. 6 and yield the anticipated linear behavior.

- *Approach* (ii) combines the local force probe measurement with measurements of the 2D beam profile using the Faraday array. As already shown in Fig. 3, the RIT-4 expels ions into a solid angle region of rotational symmetry about the thruster's cylindrical axis. Furthermore, the beam profile hardly changes with the propellant used, i.e., is virtually the same for krypton and xenon. Figure 5(a) shows beam profiles with xenon as a propellant for beam currents of 5 mA (black line), 15 mA (red dashed line), and 25 mA (blue dots). The dependence of the beam profile on the beam current is almost negligible. The normalized beam profile can be well fitted by a Gaussian-like line shape given by

$$\Phi(r) = \exp\left(-\frac{r^2}{2\sigma^2}\right), \tag{11}$$

where r denotes the distance from the central axis in cylindrical coordinates and the standard deviation σ is a measure for the linewidth of the distribution. In the case of the Gaussian profile, 95.4% of the area below the curve lies within the 4σ-interval centered at $r = 0$.

As an example, we have plotted in Fig. 5(a) the fitted curve together with the measurements for 15 mA beam current. Experimental data and fitted curve virtually cannot be distinguished. Similar quality of the fitting can be obtained for other beam currents [not shown for the experimental data of 5–25 mA beam current in Fig. 5(a)].

We define the angle of divergence α_{div} based on the 4σ-interval. For this purpose, we assume that the beam profile detected originates from a virtual point source located at distance L from the detection plane [see Fig. 5(b)]. The distance L can be derived from the distance l between the grid system and the detection plane and the diameter D of the grid system by simple geometric considerations. It holds

$$\alpha_{\mathrm{div}} = \arctan\left(\frac{2\sigma - \frac{D}{2}}{l}\right), \qquad L = l + \frac{D}{2\tan(\alpha_{\mathrm{div}})}. \tag{12}$$

Fitting the beam profiles for all beam currents measured and for both propellants with Gaussian profiles and deriving the corresponding divergence angles, we found that all values of α_{div} are in the range of $16° \pm 0.3°$.

Based on the knowledge of the beam profile, the total thrust can be determined from a local thrust measurement using the force probe as follows: The current density $j(r)$ in the detection plane corresponding to the beam profile at $z = l$ can be written as $j(r) = j(0)\Phi(r)$ where $j(0) = \frac{I_{\mathrm{target}}}{A_{\mathrm{target}}}$ of the force probe positioned at the center of the ion beam (at $r = 0$). Furthermore, the area density of the thrust per current density at $r = 0$ and $z = l$ is given by $\rho(0) = \frac{\Delta T/A_{\mathrm{target}}}{I_{\mathrm{target}}/A_{\mathrm{target}}} = \frac{\Delta T}{I_{\mathrm{target}}}$, where ΔT is the thrust increment measured by the force probe. Taking into account that the thrust contribution of an ion emitted by the virtual point source arriving at the detection plane at a distance r from the central axis is smaller as only its momentum component to the central axis contributes to the total thrust, it holds that $\rho(r) = \rho(0)\cos\beta(r)$ where $\beta(r) = \arctan(\frac{r}{L})$.

In this approximation, the total thrust T is given by the following integration:

$$\begin{aligned} T &= \int_0^\infty 2\pi r\rho(r)j(r)\,dr \\ &= j(0)\rho(0)\int_0^\infty 2\pi r\Phi(r)\cos\beta(r)\,dr \\ &\approx j(0)\rho(0)\int_0^{2\sigma} 2\pi r\Phi(r)\cos\beta(r)\,dr. \end{aligned} \tag{13}$$

The prefactor can be expressed solely by the local properties of the force probe as

$$j(0)\rho(0) = \frac{I_{\mathrm{target}}}{A_{\mathrm{target}}}\frac{\Delta T}{I_{\mathrm{target}}} = \frac{\Delta T}{A_{\mathrm{target}}}. \tag{14}$$

The total thrust is then given as

$$T \approx \frac{\Delta T}{A_{\mathrm{target}}}\int_0^{2\sigma} 2\pi r\Phi(r)\cos\beta(r)\,dr. \tag{15}$$

In this *case* (ii *a*), CEX effects along the thruster axis do not need to be accounted for as long as one assumes that that neutrals generated by CEX contribute to ΔT as the corresponding ions would have done.

Alternatively, one may express $j(0)$ by the beam current I_{beam} at $z = l$ which in turn can be related to $I_{\mathrm{beam}}(z = 0)$ by Eq. (9) establishing a dependence on the average neutral gas density n_{g} and the CEX processes between grid system and force plate. The beam current $I_{\mathrm{beam}}(z = 0)$ in the case of RIT-type thrusters is determined by the difference between the current of the screen grid and the current of the acceleration grid and thus measured directly. It holds in this *case* (ii *b*) that

$$j(0) \approx \frac{I_{\mathrm{beam}}(z = l)}{\int_0^{2\sigma} 2\pi r\Phi(r)\,dr}, \tag{16}$$

yielding

$$\begin{aligned} T &\approx \frac{I_{\mathrm{beam}}(z = l)}{\int_0^{2\sigma} 2\pi r\Phi(r)\,dr}\frac{\Delta T}{I_{\mathrm{target}}}\int_0^{2\sigma} 2\pi r\Phi(r)\cos\beta(r)\,dr \\ &= \frac{I_{\mathrm{beam}}(z = 0)\exp(-\sigma_{\mathrm{CEX}}^{\mathrm{Xe}} n_{\mathrm{g}} l)}{\int_0^{2\sigma} 2\pi r\Phi(r)\,dr}\frac{\Delta T}{I_{\mathrm{target}}} \\ &\quad \times \int_0^{2\sigma} 2\pi r\Phi(r)\cos\beta(r)\,dr. \end{aligned} \tag{17}$$

Furthermore, the comparison of *cases* (ii *a*) and (*ii b*) for the same settings yields the average neutral gas density n_{g} between the grid and the force plate as

$$n_{\mathrm{g}} \approx -\frac{1}{\sigma_{\mathrm{CEX}}^{\mathrm{Xe}} l}\ln\left(\frac{I_{\mathrm{target}}}{A_{\mathrm{target}} I_{\mathrm{beam}}(z = 0)}\int_0^{2\sigma} 2\pi r\Phi(r)\,dr\right). \tag{18}$$

Approach (iii): Another theoretical possibility to obtain the total thrust T is to correct the ideal thrust T_{ideal} given by Eq. (5) for beam divergence. Based on the beam profile measurement, one obtains[15]

© Author(s) 2022

$$T = T_{\text{ideal}} \frac{\int_0^{\infty} 2\pi r \Phi(r) \cos\beta(r)\, dr}{\int_0^{\infty} 2\pi r \Phi(r)\, dr} \approx T_{\text{ideal}} \frac{\int_0^{2\sigma} 2\pi r \Phi(r) \cos\beta(r)\, dr}{\int_0^{2\sigma} 2\pi r \Phi(r)\, dr}, \quad (19)$$

where again the factor $\cos\beta(r)$ accounts for the fact that, in rotational symmetry, the transverse momentum components of all ions arriving at distance r from the central axis in the detection plane add up to zero, thus canceling each other. A calculation of T_{ideal} by Eq. (5) requires the knowledge of the operational parameters—beam current $I_{\text{beam}}(z = 0)$ and U_{tot}. Under the operational conditions employed in the experiments, plasma and floating potential sum up to 45 V. Together with the acceleration voltage U_{acc} = 1000 V at the grids, a total acceleration voltage of U_{tot} = 1045 V arises.

In what follows, we will compare the determination of the thrust T by the three approaches: by the direct measurement approach (i) using the thrust balance, by the indirect approach (ii a) using the local results of force probe and beam profile measurement according to Eq. (15), and the indirect more "theoretical" approach (iii) carrying out a divergence correction of the ideal thrust as given in Eq. (19).

Figure 6(a) depicts the experimental thrust values vs beam current $I_{\text{beam}}(z = 0)$ obtained by the three approaches. The green solid line represents the thrust values determined by approach (iii). A perfect linear dependence arises as the ideal thrust is proportional to the beam current [see Eq. (5)] and as we assume the same beam profile independent of the total beam current. The thrust values measured with the thrust balance [approach (i)] given by the blue circles are somewhat lower, but in rather good agreement with those of approach (iii). The values of the more theoretical approach (iii) are anticipated to present a kind of upper boundary of the thrust as the energy of the ions of the beam is not described by a distribution of ion energies, but is set to the anticipated maximum ion energy for all ions, i.e., 1045 eV. In particular, at lower thrusts, the deviation of the thrust values obtained with the thrust balance is somewhat larger. In this context, it should be noted that the lowest thrust detectable by the thrust balance is about 250 μN. At these low thrusts, friction effects within the thrust balance, which inherently lower the measured thrust value, play a greater role than at higher thrusts. The origin of the error bars of the thrust balance measurement was determined as discussed above. The thrust values derived by the force probe measurements according to (ii a) given by the black symbols lie in the same range as those of the other two approaches. The data points show a clear trend but deviate from a straight line. At low thrusts, the data points are significantly lower than the green line and then approach and even cross the green line at high thrusts, i.e., the measured thrust is higher than the upper boundary given by approach (iii). Two effects are responsible for the observed behavior. First, there are CEX effects. This becomes clear when analyzing the neutral gas density between the thruster and the force plate according to Eq. (18). The values as a function of ion beam current $I_{\text{beam}}(z = 0)$ are depicted in Fig. 6(b) and show the anticipated behavior. The propellant mass flow was kept constant throughout the experiments. In this situation, pressure in front of the grid system will depend on the extracted beam current. In particular, it will decrease with increasing beam current as the ion beam pushes the neutrals aside. It starts off in the range of 10^{18} m^{-3} and then at I_{beam} = 30 mA approaches almost zero. If one assumes, as a simplification, that the neutral gas density between thruster and detection systems, i.e., Faraday array and force probe, is constant, it becomes clear that, in the presence of CEX effects, the thrust should be underestimated due to the geometry of the Faraday array measurement. The distance between the center of the grid and central Faraday cup of the array increases with increasing r as $\sqrt{r^2 + l^2}$, i.e., more ions are converted into fast neutrals that contribute to the thrust but not to the current density $j(r)$. Thus, $j(r)$ is underestimated by the Faraday measurement with increasing r. This results in an underestimation of the total thrust T derived by Eq. (15) as $\rho(0)$ is kept constant. This explains the behavior of the thrust values determined by approach (ii a) at low beam currents. However, CEX effects cannot be the only effect causing deviations; otherwise, the data points at high beam currents (low n_g) should approach the green line from below. The crossing observed must be due to another effect. This second effect arises due to the difficulty in positioning the force plate of the force probe and the detection plane of the Faraday array exactly at the same distance l from the grid. Positioning the Faraday array, a $\Delta l \approx 1$ cm further away from the grid than the force probe would already lead to an overestimation of $j(0)$ by almost 10%, i.e., sufficient to cause the crossing of the green curve observed.

IV. CONCLUSIONS

The exact determination of thrust is essential for the characterization of electric propulsion systems. The data measured with conventional thrust balances are associated with large uncertainties. Therefore, it is important to develop and test other methods of thrust measurement. A viable alternative is approaches based on the use of a force probe. The force probe measures the fraction of the total thrust of the plume exerted as force on a defined target area, instead of measuring the total thrust directly via the force exerted on the thruster mounted on the thrust balance. The force on the target of the probe exerted by the plume is related to the force on the thruster via Newton's third law, i.e., momentum conservation in the plume-thruster system.

Two difficulties arise when using a force probe approach for assessing the thrust of an ion engine. First, the force probe measurement is a local measurement and records only the force due to a fraction of the ion beam. Second, care must be taken to correct for CEX effects occurring when the ion beam traverses the distance between the thruster and force probe. In our approach (ii a) that correlates a local incremental thrust measurement with the ion beam profile, CEX effects are hard to avoid but may be well estimated. Both difficulties may be entirely overcome by spatial scanning of the force probe in order to obtain the total thrust as a sum of the incremental thrust measurements. However, this requires further optimization of the force probe system in terms of a reliable *in situ* calibration at each measurement position and a reliable and fast movement of the force probe system in front of the thruster inside the vacuum chamber. It is worth noting that the calibration routine of the force probe can be further optimized. For example, it is possible to mount a voice coil at the ceramic rod and use the coil to generate a force on the rod. Thus, this voice coil enables an *in situ* calibration where the chosen step width ΔT during calibration solely depends on the accuracy of the power supply used for driving the voice coil. If these challenges are

© Author(s) 2022

overcome, one may take real advantage of the promising properties of the force probe. For example, its thrust resolution is independent of the ratio of thrust to thruster weight T/W or power and propellant lines necessary for operating the thruster do not affect the force probe measurement, in contrast to the thrust balance measurement.

In conclusion, accurate thrust measurements of ion thrusters and other EP systems remain challenging. Using indirect force probe approaches instead of direct approaches based on thrust balances may offer considerable advantages in the future because there are no power supply-line effects disturbing the measurement, the thruster does not have to be mounted on the measurement device, the weight of the thruster does not matter, and the measurement approach is very sensitive to small force and current changes. In our experiment with an RIT thruster, the direct comparison of the force probe and the thrust balance shows good agreement but is still affected by charge exchange effects between ions and neutrals within the beam. However, the magnitude of these effects may be estimated quantitatively. In conclusion, indirect thrust measurements based on force probes are already suitable alternatives to conventional thrust balance measurements.

ACKNOWLEDGMENTS

This work was supported by the framework of the MINOTOR project that has received funding from the European Union's Horizon 2020 research and innovation program under Grant Agreement No. 730028.

The authors also gratefully acknowledge funding by the Federal State of Hessen and the European Regional Development Fund (Grant No. ERDF/EFRE 2014–2020) (Vorhaben: "Innovationslabor: Physik unter harschen Bedingungen," Grant No. FKZ: FPG991 0002/2019).

AUTHOR DECLARATIONS

Conflict of Interest

The authors have no conflicts to disclose.

DATA AVAILABILITY

The data that support the findings of this study are available within the article.

REFERENCES

[1] S. Mazouffre, "Electric propulsion for satellites and spacecraft: Established technologies and novel approaches," Plasma Sources Sci. Technol. **25**(3), 033002 (2016).

[2] K. Holste, P. Dietz, S. Scharmann, K. Keil, T. Henning, D. Zschätzsch, M. Reitemeyer, B. Nauschütt, F. Kiefer, F. Kunze, J. Zorn, C. Heiliger, N. Joshi, U. Probst, R. Thüringer, C. Volkmar, D. Packan, S. Peterschmitt, K.-T. Brinkmann, H.-G. Zaunick, M. H. Thoma, M. Kretschmer, H. J. Leiter, S. Schippers, K. Hannemann, and P. J. Klar, "Ion thrusters for electric propulsion: Scientific issues developing a niche technology into a game changer," Rev. Sci. Instrum. **91**(6), 061101 (2020).

[3] J. E. Polk, A. Pancotti, T. Haag, S. King, M. Walker, J. Blakely, and J. Ziemer, "Recommended practice for thrust measurement in electric propulsion testing," J. Propul. Power **33**(3), 539–555 (2017).

[4] T. Moeller and K. A. Polzin, "Thrust stand for vertically oriented electric propulsion performance evaluation," Rev. Sci. Instrum. **81**(11), 115108 (2010).

[5] K. A. Polzin, T. E. Markusic, B. J. Stanojev, A. DeHoyos, and B. Spaun, "Thrust stand for electric propulsion performance evaluation," Rev. Sci. Instrum. **77**(10), 105108 (2006).

[6] D. Frollani, M. Coletti, and S. B. Gabriel, "A thrust balance for low power hollow cathode thrusters," Meas. Sci. Technol. **25**(6), 065902 (2014).

[7] M. Gamero-Castaño, "A torsional balance for the characterization of microNewton thrusters," Rev. Sci. Instrum. **74**(10), 4509–4514 (2003).

[8] T. W. Haag, "Thrust stand for pulsed plasma thrusters," Rev. Sci. Instrum. **68**(5), 2060–2067 (1997).

[9] M. R. Anselmo and R. I. Marques, "Torsional thrust balance for electric propulsion application with electrostatic calibration device," Meas. Sci. Technol. **30**(5), 055903 (2019).

[10] K. G. Xu and M. L. R. Walker, "High-power, null-type, inverted pendulum thrust stand," Rev. Sci. Instrum. **80**(5), 055103 (2009).

[11] P. Daponte, R. Rassa, S. Debei, S. Dyer, P. Carbone, M. Pisani, C. Ferrero, P. Tavella, F. Ongaro, K. Chance, G. Nicolella, C. Paoli, and G. Lavacca, in *4th IEEE International Workshop on Metrology for AeroSpace: Padua, Italy, June 21-23, 2017* (IEEE, Piscataway, NJ, 2017).

[12] T. Trottenberg, T. Richter, and H. Kersten, "Measurement of the force exerted on the surface of an object immersed in a plasma," Eur. Phys. J. D **69**(3), 91 (2015).

[13] T. Trottenberg, A. Spethmann, and H. Kersten, "An interferometric force probe for beam diagnostics and the study of sputtering," EPJ Tech. Instrum. **5**(1), 3 (2018).

[14] M. Becker, M. Gies, A. Polity, S. Chatterjee, and P. J. Klar, "Materials processing using radio-frequency ion-sources: Ion-beam sputter-deposition and surface treatment," Rev. Sci. Instrum. **90**(2), 023901 (2019).

[15] A. Michael and A. J. L. Lieberman, *Principles of Plasma Discharges and Materials Processing* (Wiley, 2005).

[16] A. Spethmann, T. Trottenberg, and H. Kersten, "Measurement and simulation of forces generated when a surface is sputtered," Phys. Plasmas **24**(9), 093501 (2017).

[17] M. I. Patino and R. E. Wirz, "Electron emission from carbon velvet due to incident xenon ions," Appl. Phys. Lett. **113**(4), 041603 (2018).

[18] N. Matsunami, Y. Yamamura, Y. Itikawa, N. Itoh, Y. Kazumata, S. Miyagawa, K. Morita, R. Shimizu, and H. Tawara, "Energy dependence of the ion-induced sputtering yields of monatomic solids," At. Data Nucl. Data Tables **31**(1), 1–80 (1984).

[19] C. Steinbrüchel, "A simple formula for low-energy sputtering yields," Appl. Phys. A **36**(1), 37–42 (1985).

[20] P. Chabert, J. A. Monreal, J. Bredin, L. Popelier, and A. Aanesland, "Global model of a gridded-ion thruster powered by a radiofrequency inductive coil," Phys. Plasmas **19**(7), 073512 (2012).

[21] M. L. Hause, B. D. Prince, and R. J. Bemish, "Krypton charge exchange cross sections for Hall effect thruster models," J. Appl. Phys. **113**(16), 163301 (2013).

[22] J. S. Miller, S. H. Pullins, D. J. Levandier, Y.-h. Chiu, and R. A. Dressler, "Xenon charge exchange cross sections for electrostatic thruster models," J. Appl. Phys. **91**(3), 984–991 (2002).

© Author(s) 2022